

## EPR Evidence for Co(IV) Species Produced During Water Oxidation at Neutral pH

J. Gregory McAlpin,<sup>†</sup> Yogesh Surendranath,<sup>‡</sup> Mircea Dincă,<sup>‡</sup> Troy A. Stich,<sup>†</sup> Sebastian A. Stoian,<sup>‡</sup> William H. Casey,<sup>\*,†</sup> Daniel G. Nocera,<sup>\*,‡</sup> and R. David Britt<sup>\*,†</sup>

Department of Chemistry, University of California, 1 Shields Avenue, Davis, California 95616-0935, and  
Department of Chemistry, Massachusetts Institute of Technology, 77 Massachusetts Avenue, Cambridge,  
Massachusetts 02139-4307

Received February 15, 2010; E-mail: whcasey@ucdavis.edu; nocera@mit.edu; rdbritt@ucdavis.edu

Electrochemical water splitting is the preeminent method for storing solar energy in the form of chemical fuels.<sup>1,2</sup> Water splitting involves the four-electron–four-proton oxidation of water to oxygen and the reduction of the resultant protons to hydrogen. Of the two half-reactions, the oxygen evolution half-reaction is particularly demanding because it requires the distribution of multiple redox processes over a narrow potential range, the coupling of multiple proton and electron transfers, and the formation of two oxygen–oxygen bonds.<sup>3</sup> We have effected this challenging reaction in neutral water with a heterogeneous Co–Pi catalyst formed from the electrolysis of aqueous Co(II) in phosphate-buffered, neutral-pH electrolyte solutions.<sup>4–6</sup> This catalyst enhances the efficiency of electrochemical water oxidation when deposited on inert fluorine tin oxide (FTO) or indium tin oxide (ITO) anodes and enhances the efficiency of photoelectrochemical water oxidation when deposited on ZnO and Fe<sub>2</sub>O<sub>3</sub> photoanodes.<sup>7,8</sup> An understanding of the mechanism of water oxidation intimately depends on detailed characterization of the catalyst in an active form.

The mechanism of catalytic water oxidation at Co(II,III) spinels and perovskites has been studied extensively under alkaline conditions (pH > 13).<sup>9–13</sup> For these oxides, it is believed that polarization induces the formation of surface Co(IV) sites, which serve as key intermediates in the pathway for O<sub>2</sub> evolution.<sup>9–13</sup> Despite the ubiquity of putative Co(IV) intermediates in the literature on cobalt oxide-catalyzed water oxidation, neither *in situ* nor *ex situ* spectroscopic characterization of Co(IV) species in these systems has been reported to date, leaving a definitive assignment ambiguous. Herein, we provide electron paramagnetic resonance (EPR) evidence of the presence of Co(IV) species formed in Co–Pi films during electrocatalytic water oxidation.

For this study, Co–Pi catalyst films were electrodeposited onto large FTO plates ( $\sim 200$  cm<sup>2</sup>) by bulk electrolysis of aqueous 0.5 mM solutions of Co(NO<sub>3</sub>)<sub>2</sub> in 0.1 M potassium phosphate (pH 7.0) (Pi electrolyte) at potentials greater than 1.0 V (all potentials in this study are reported vs NHE).<sup>5</sup> Electrolysis of Co(II)-containing Pi electrolyte solutions for 12 h at a potential of 1.34 V led to a thick brown/black catalyst film. Upon conclusion of electrolysis, the film was dried and manually removed from the electrode surface to yield  $\sim 5$  mg of black powder that was immediately loaded into an EPR tube and then frozen and stored at 77 K.

The continuous-wave (CW) X-band EPR spectrum of this frozen catalyst is shown in Figure 1b. A broad resonance at  $g_{\text{eff}} \approx 5$  along with a broad derivative line shape at  $g_{\text{eff}} = 2.27$  is observed. The feature at  $g_{\text{eff}} \approx 5$  is reminiscent of EPR spectra measured for many Co(II)-containing compounds, including Co<sub>3</sub>O<sub>4</sub>, Co<sub>3</sub>(PO<sub>4</sub>)<sub>2</sub>, and a

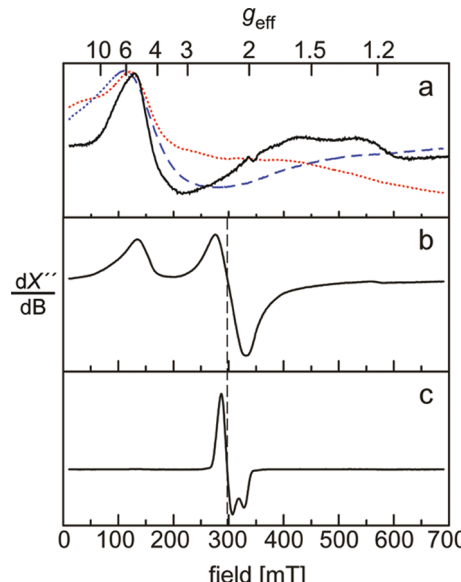


**Figure 1.** CW X-band EPR spectra of (a) the frozen electrolysis solution (black solid curve), Co<sub>3</sub>(PO<sub>4</sub>)<sub>2</sub> (red dotted curve), Co<sub>3</sub>O<sub>4</sub> (blue dashed curve); (b) Co–Pi catalyst films deposited at 1.34 V; and (c) [Co<sub>4</sub>O<sub>4</sub>(C<sub>5</sub>H<sub>5</sub>N)<sub>4</sub>(CH<sub>3</sub>CO<sub>2</sub>)<sub>4</sub>](ClO<sub>4</sub>). The vertical dotted line indicates  $g = 2.27$ .  $T = 5.7$  K; microwave power = 1.02 mW.

frozen solution of the electrodeposition bath (Figure 1a). Each of these examples exhibits a broad, prominent peak with a maximum at  $g_{\text{eff}} = 5$ –8. On the basis of this similarity, we have assigned the  $g_{\text{eff}} \approx 5$  feature in the catalyst to an  $S = \frac{3}{2}$  Co(II) species in the material.

Results from X-ray absorption spectroscopy (XAS) studies suggest that Co–Pi consists of Co–oxido clusters composed of edge-sharing CoO<sub>6</sub> octahedra.<sup>14,15</sup> This geometry should enforce a low-spin, EPR-silent configuration on Co(III) centers in the film. Examples of high-spin Co(III) species are rare and exist only with weak-field ligands.<sup>16,17</sup> Furthermore, the EPR spectrum of the model system, Co(II,III) spinel (Co<sub>3</sub>O<sub>4</sub>), does not exhibit any prominent features attributable to Co(III). Thus, we are confident that all of the Co(III) sites in the film are indeed low-spin. We expect this low-spin configuration to be preserved upon further cobalt-centered oxidation to yield  $S = \frac{1}{2}$  Co(IV) species.<sup>18</sup>

To aid in the assignment of the  $g_{\text{eff}} = 2.27$  feature, we investigated the EPR properties of a unimolecular Co-containing cubane, [Co<sub>4</sub>O<sub>4</sub>(C<sub>5</sub>H<sub>5</sub>N)<sub>4</sub>(CH<sub>3</sub>CO<sub>2</sub>)<sub>4</sub>](ClO<sub>4</sub>) (1).<sup>19</sup> The Co<sub>4</sub>O<sub>4</sub> core of this model compound is composed of one Co(IV) and three Co(III) centers and is structurally similar to the cuboidal framework believed to exist in the catalyst film.<sup>14,15</sup> The cubane exhibits an

<sup>†</sup> University of California, Davis.

<sup>‡</sup> Massachusetts Institute of Technology.

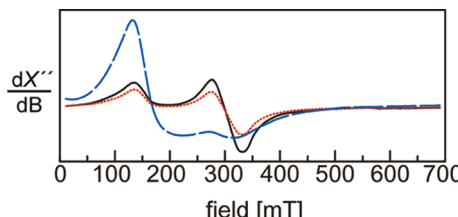


**Figure 2.** CW X-band EPR spectra of Co–Pi catalyst films deposited from aqueous 0.5 mM  $\text{Co}(\text{NO}_3)_2$  solutions in 0.1 M Pi electrolyte (pH 7.0) at 1.03 V (blue dashed curve), 1.14 V (red dotted curve), and 1.34 V (black solid curve). Spectra were scaled by the amount of cobalt in each sample, as measured by atomic absorption spectroscopy.  $T = 5.7$  K; microwave power = 1.02 mW.

axial EPR signal (Figure 1c) with  $g_{\perp} = 2.33$  and  $g_{\parallel} = 2.06$ , diagnostic of an  $S = \frac{1}{2}$  system arising from the low-spin Co(IV) center and the three EPR-silent Co(III) centers. Both the model cubane and the catalyst film share a zero-crossing point at  $g = 2.27$ , as indicated by the vertical dashed line in Figure 1b,c.

Furthermore, we examined the potential dependence of the EPR signals observed in Co–Pi films. The EPR spectra of films prepared at potentials of 1.03, 1.14, and 1.34 V are shown in Figure 2. For the film prepared at 1.03 V, where the rate of water oxidation is negligible, a large Co(II) feature together with a small signal at  $g_{\text{eff}} = 2.27$  is observed. For films prepared at 1.14 and 1.34 V, where the rates of water oxidation are significant, the Co(II) feature is dramatically diminished, with an associated rise in intensity of the  $g_{\text{eff}} = 2.27$  feature. Indeed, this increase in signal intensity between the 1.14 and 1.34 V samples parallels an increase in the rate of water oxidation by greater than 2 orders of magnitude.

The progressive rise in the intensity of the  $g_{\text{eff}} = 2.27$  feature as the potential is increased, together with its similarity to the signal observed in the cubane model compound, provides strong evidence for the assignment of the  $g_{\text{eff}} = 2.27$  signal to low-spin Co(IV)-containing species. Moreover, the potential dependence of this signal suggests that it arises predominantly from species generated during electrocatalytic water oxidation. Consistent with the high oxidizing power of Co(IV) species in the catalyst, the observed Co(IV) signal decays over the course of minutes at room temperature even in the dry, isolated film (Figure S1 in the Supporting Information).

To estimate the populations of Co(IV) spins in catalysts prepared at 1.14 and 1.34 V, the spectrum of the material grown at 1.03 V was scaled to the intensity of the Co(II) feature in each of the high-potential spectra. Subtraction of the low-potential spectrum from the high-potential spectra permitted the Co(II) feature to be removed and revealed a spectrum consisting predominantly of the  $S = \frac{1}{2}$  Co(IV) signal (Figure S2). From double integration of this signal relative to that of an  $S = \frac{1}{2}$  spin standard,  $\text{Cu}(\text{EDTA})(\text{SO}_4)$ , we calculated that 3 and 7% of all the Co centers in the films grown at 1.14 and 1.34 V, respectively, were in this Co(IV) oxidation state. In quantitating Co(IV) spins in the solid-state catalyst with a frozen-solution spin standard, we assumed that neighboring diamagnetic Co(III) ions provided a sufficiently magnetically dilute environment that spin–spin interactions that could have distorted the spectrum were negligible (see the Supporting Information).

In the foregoing discussion, changes in the redox speciation of the films were induced by growing the films at elevated potentials where water oxidation and film formation occur simultaneously. For this situation, we expect that some of the Co(IV) species generated during catalytic turnover may be trapped in the film by newly formed catalyst layers. This trapping would inhibit quenching of Co(IV) intermediates, thereby permitting their observation in an ex-situ experiment. To test this hypothesis, two electrodes were

prepared in an identical manner at 1.04 V, below the onset of water oxidation catalysis. Catalyst material was isolated from the first electrode immediately following deposition, whereas the second electrode was transferred to Co-free Pi electrolyte solution and electrolyzed at a potential sufficient for water oxidation catalysis (>1.2 V). Time points ranging from 5 min to 12 h were investigated. The catalyst performing water oxidation without additional film formation exhibited a decrease in the Co(II) signal concomitant with an increase in the Co(IV) signal (Figure S3). These changes in redox speciation are similar to those observed for films electrodeposited at 1.21 V under identical conditions (Figure S4), suggesting that the  $g_{\text{eff}} = 2.27$  signal is due at least in part to redox transformations that occur in the material over the course of water oxidation catalysis. We note that the  $g_{\text{eff}} = 2.27$  signal formed after only 5 min of water oxidation catalysis has >60% of the amplitude of that observed after 12 h of electrolysis.

In conclusion, we have shown that Co–Pi catalyst films exhibit paramagnetic signals corresponding to populations of both Co(II) and Co(IV) species. As the deposition voltage is increased to a value sufficient to support water oxidation catalysis, the population of the Co(IV) species rises, with an attendant decrease in the proportion of the Co(II) species. The changes in the redox speciation of the film can also be induced in part by prolonged water oxidation catalysis in the absence of additional film formation. These results provide spectroscopic evidence for the formation of Co(IV) species during water oxidation catalysis by these thin films and open the door to the implementation of in situ and double-resonance EPR techniques aimed at characterizing the coordination environment of the active Co(IV) species.

**Acknowledgment.** This research was supported by NSF CCI Powering the Planet Grants CHE-0802907 and CHE-0947829 and grants from the NSF (CHE-0533150, CHE-0939178, EAR0814242), the U.S. Department of Energy (DE-FG02-05ER15693), and the Chesonis Family Foundation. Y.S. gratefully acknowledges the NSF for a predoctoral fellowship.

**Supporting Information Available:** Full experimental details and synthetic details for 1. This information is available free of charge via the Internet at <http://pubs.acs.org>.

## References

- Lewis, N. S.; Nocera, D. G. *Proc. Natl. Acad. Sci. U.S.A.* **2006**, *103*, 15729.
- Nocera, D. G. *Inorg. Chem.* **2009**, *48*, 10001.
- Betley, T. A.; Wu, Q.; Voorhis, T. V.; Nocera, D. G. *Inorg. Chem.* **2008**, *47*, 1849.
- Kanan, M. W.; Nocera, D. G. *Science* **2008**, *321*, 1072.
- Surendranath, Y.; Dincă, M.; Nocera, D. G. *J. Am. Chem. Soc.* **2009**, *131*, 2615.
- Lutterman, D. A.; Surendranath, Y.; Nocera, D. G. *J. Am. Chem. Soc.* **2009**, *131*, 3838.
- Zhong, D. K.; Sun, J.; Inumaru, H.; Gamelin, D. R. *J. Am. Chem. Soc.* **2009**, *131*, 6086.
- Steinmiller, E. M. P.; Choi, K.-S. *Proc. Natl. Acad. Sci. U.S.A.* **2009**, *106*, 20633.
- Bockris, J. O.; Otagawa, T. *J. Phys. Chem.* **1983**, *87*, 2960.
- Lyons, M. E. G.; Brandon, M. P. *Int. J. Electrochem. Sci.* **2008**, *3*, 1425.
- Castro, E. B.; Gervasi, C. A. *Int. J. Hydrogen Energy* **2000**, *25*, 1163.
- Conway, B. E.; Liu, T. C. *Ber. Bunsen-Ges. Phys. Chem.* **1987**, *91*, 461.
- Singh, R. N.; Koenig, J.-F.; Poillerat, G.; Chartier, P. *J. Electrochem. Soc.* **1990**, *137*, 1408.
- Risch, M.; Khare, V.; Zaharieva, I.; Gerencser, L.; Chernev, P.; Dau, H. *J. Am. Chem. Soc.* **2009**, *131*, 6936.
- Kanan, M. W.; Yano, J.; Surendranath, Y.; Dincă, M.; Yachandra, V. K.; Nocera, D. G. *J. Am. Chem. Soc.*, submitted for publication.
- Cotton, F. A.; Meyers, M. D. *J. Am. Chem. Soc.* **1960**, *82*, 5023.
- Kojima, K.; Matsuda, J.; Kojima, N.; Ban, T.; Tsujikawa, I. *Bull. Chem. Soc. Jpn.* **1987**, *60*, 3213.
- Even if the Co(III) ions were somehow in a high-spin electron configuration, we would not expect to observe a signal in the  $g = 2$  spectral region for these non-Kramers centers.
- Chakrabarty, R.; Bora, S. J.; Das, B. K. *Inorg. Chem.* **2007**, *46*, 9450.

JA101334